ACSNANO

www.acsnano.org

ARTICLE

Gallium Nanodroplets are Anti-Inflammatory without Interfering with Iron Homeostasis

Chengchen Zhang, Biyao Yang, Joanna M. Biazik, Richard F. Webster, Wanjie Xie, Jianbo Tang, Francois-Marie Allioux, Roozbeh Abbasi, Maedehsadat Mousavi, Ewa M. Goldys, Kristopher A. Kilian, Rona Chandrawati, Dorna Esrafilzadeh,* and Kourosh Kalantar-Zadeh*

Cite This: https://doi.org/10.1021/acsnano.1c10981

Read Online

ACCESS | Metrics & More | Article Recommendations | Supporting Information

ABSTRACT: Gallium (Ga) compounds, as the source of Ga ions (Ga^{3+}), have been historically used as anti-inflammatories. Currently, the widely accepted mechanisms of the anti-inflammatory effects for Ga^{3+} are rationalized on the basis of their similarities to ferric ions (Fe^{3+}), which permits Ga^{3+} to bind with Fe-binding proteins and subsequently disturbs the Fe homeostasis in the immune cells. Here in contrast to the classic views, our study presents the mechanisms of Ga as anti-inflammatory by delivering Ga nanodroplets (GNDs) into lipopolysaccharide-induced macrophages and exploring the processes. The GNDs show a selective inhibition of nitric oxide (NO) production without affecting the accumulation of pro-inflammatory mediators. This is explained by GNDs disrupting the synthesis of inducible NO synthase in the activated macrophages by upregulating the levels of eIF2α phosphorylation, without interfering with the Fe homeostasis. The Fe^{3+} transferrin receptor-independent endocytosis of GNDs by the cells prompts a fundamentally different mechanism as anti-inflammatories in comparison to that imparted by Ga^{3+}. This study reveals the fundamental molecular basis of GND−macrophage interactions, which may provide additional avenues for the use of Ga for anti-inflammatory and future biomedical and pharmaceutical applications.

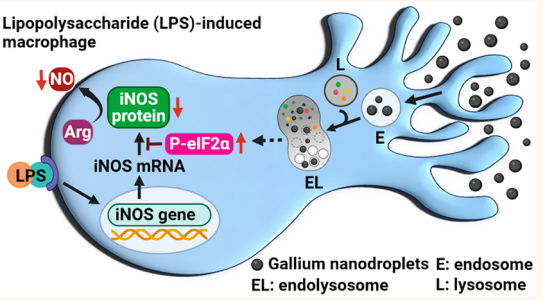

KEYWORDS: *liquid metal, gallium nanodroplet, anti-inflammatory, iron homeostasis, nitric oxide*

1. INTRODUCTION

Gallium (Ga) compounds, as the source of Ga ions (Ga^{3+}), have historically been shown to present anti-inflammatory effects by modulating the production of nitric oxide (NO) and pro-inflammatory cytokines from the activated immune cells.[1−3] Currently, proposed mechanisms of the anti-inflammatory effects shown in Ga^{3+} are rationalized on the basis of their similarities with ferric ions (Fe^{3+}), which permits Ga^{3+} to act as a nonfunctional Fe^{3+} mimetic to bind with Fe-binding proteins.[4] Substitution of Ga^{3+} prohibits the native protein functions and further disturbs Fe homeostasis in the immune cells.[5] However, Fe is an essential growth factor for the proliferation and differentiation of all cells.[6] As such, the ability of Ga^{3+} binding to those proteins, especially transferrin, can disrupt Fe homeostasis in untargeted cells and therefore render adverse downstream effects on certain Fe-dependent processes.[5]

With the progress of nanotechnology, it has become more possible to deliver and release drugs in specific sites with the assistance of nanomaterials.[7−9] In particular, recent reports have shown the peculiarity of Ga nanodroplets (GNDs) in such applications.[10−13] Gallium bulk and Ga-based alloys, in their liquid form, can be mechanically broken down into smaller submicron or nanodroplets.[14] These droplets can interact with living cells,[15] and they have been incorporated in biomedical applications including drug delivery,[16−18] cancer therapy,[19−21] medical imaging,[22,23] ion channel regulation,[22] biosensing,[24] and pathogen treatment,[25−27] by taking advantage of their properties such as low cytotoxicity and high thermal and electrical conductivities and their ability to respond to electric and magnetic fields[6] and infrared (IR) stimulation.[22,28] In alignment with such demonstrations, here we investigate that delivering Ga, in the form of submicron or nanodroplets, into immune cells is potentially a promising strategy to modulate discrete signaling pathways, while avoiding the adverse effects of using traditional Ga^{3+}. It is hypothesized that the submicron or nano sized Ga particles

Received: December 10, 2021
Accepted: May 20, 2022

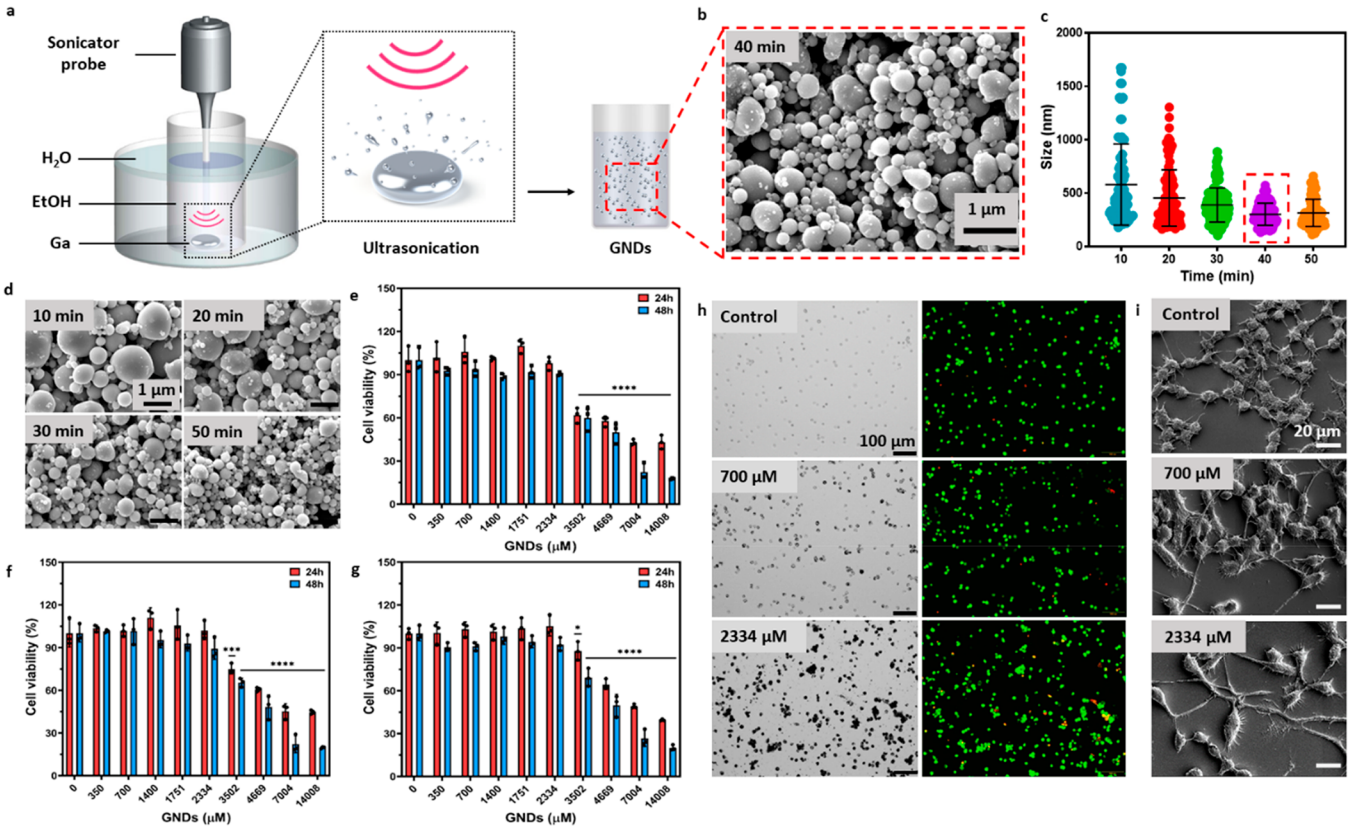

Figure 1. Preparation, morphological analyses, and biocompatibility assessments of GNDs. (a) Schematic illustration of the GNDs preparation process. (b) Representative SEM images for assessing the morphology of GNDs sonicated for 40 min. (c) Sizes of GNDs synthesized at different sonication times (from 10 to 50 min). Error bars represent s.d. of n = 100 size measurements of GNDs. (d) Representative SEM images for assessing the morphology of GNDs sonicated for 10, 20, 30, and 50 min. (e−g) Cell viability of RAW 264.7 cells exposed to different concentrations of GNDs at 24 and 48 h. GNDs were sonicated for 10 min (e), 20 min (f), and 40 min (g), respectively. Error bars represent s.d. of n = 3 replicates. (h) Representative live and dead double fluorescence staining images of RAW 264.7 cells in the present of different concentrations of GNDs for 48 h. Optical microscopy images (left) and fluorescent images show cells incubated with GNDs at different durations. Live and dead cells are shown in green and red fluorescence, respectively (right). (i) Representative SEM images of RAW 264.7 cells in the present of different concentrations of GNDs for 48 h. The control groups in (h) and (i) indicate cells in normal growth media in the absence of GNDs. $P < 0.05$ is considered as statistically significant. *$P < 0.05$, **$P < 0.01$, ***$P < 0.001$, and ****$P < 0.0001$.

may be engulfed into the cells directly, without relying on the transferrin receptor (TfR).

To investigate our hypothesis mentioned above, we designed low-dimensional Ga, in the form of nanodroplets and then delivered them into macrophages and explored their anti-inflammatory processes. Macrophages are critical for immune responses against pathogenic infections. When macrophages are exposed to molecules such as lipopolysaccharide (LPS), which is known to exist on the outer membrane of Gram-negative bacteria,[29,30] they discharge NO and pro-inflammatory cytokines including interleukin-6 (IL-6) and tumor necrosis factor-α (TNF-α).[31,32] Nitric oxide, a short-lived, small, labile, lipid-permeable free radical, mediates many biological functions, produced endogenously by immune cells during inflammation for pathogen killing.[33,34] Specifically, activated macrophages release high levels of NO for anti-infection by a NO synthase isoform known as inducible NO synthase (iNOS).[31,35] However, the role of NO is nonspecific and overproduction of NO can lead to various disorders such as tissue injuries.[36,37]

Surprisingly in our observations, the GNDs show an anti-inflammatory effect based on inhibiting NO production without affecting the accumulation of pro-inflammatory mediators, which is different from the effect of Ga^{3+}, which inhibits both. The selective inhibitory effect on NO was explained by GNDs disrupting iNOS mRNA translation to iNOS protein in the LPS-induced macrophages, without affecting the Fe homeostasis. We explore and associate the observation to the direct uptake of GNDs by macrophages, without interfering with the Fe^{3+} TfR-mediated endocytosis. These results and related mechanisms successfully verify our hypothesis and offer a base for innovative use of Ga as an anti-inflammatory agent in the future.

RESULTS AND DISCUSSION

Preparation and Characterization of GNDs. The GNDs were synthesized by a probe sonication of Ga bulk in ethanol (EtOH) as illustrated in Figure 1a, and the detailed process is provided in the Methods and Materials section. The scanning electron microscopy (SEM) images (Figure 1b,d) show spherical GNDs were synthesized successfully within sonication time from 10 to 50 min. The dimensions of GNDs (Figure 1c and Supplementary Table 1) show that a longer sonication time from 10 to 40 min produced GNDs with smaller average diameters and narrower size distributions, whereas there is no significant difference from 40 to 50 min.

https://doi.org/10.1021/acsnano.1c10981
ACS Nano XXXX, XXX, XXX−XXX

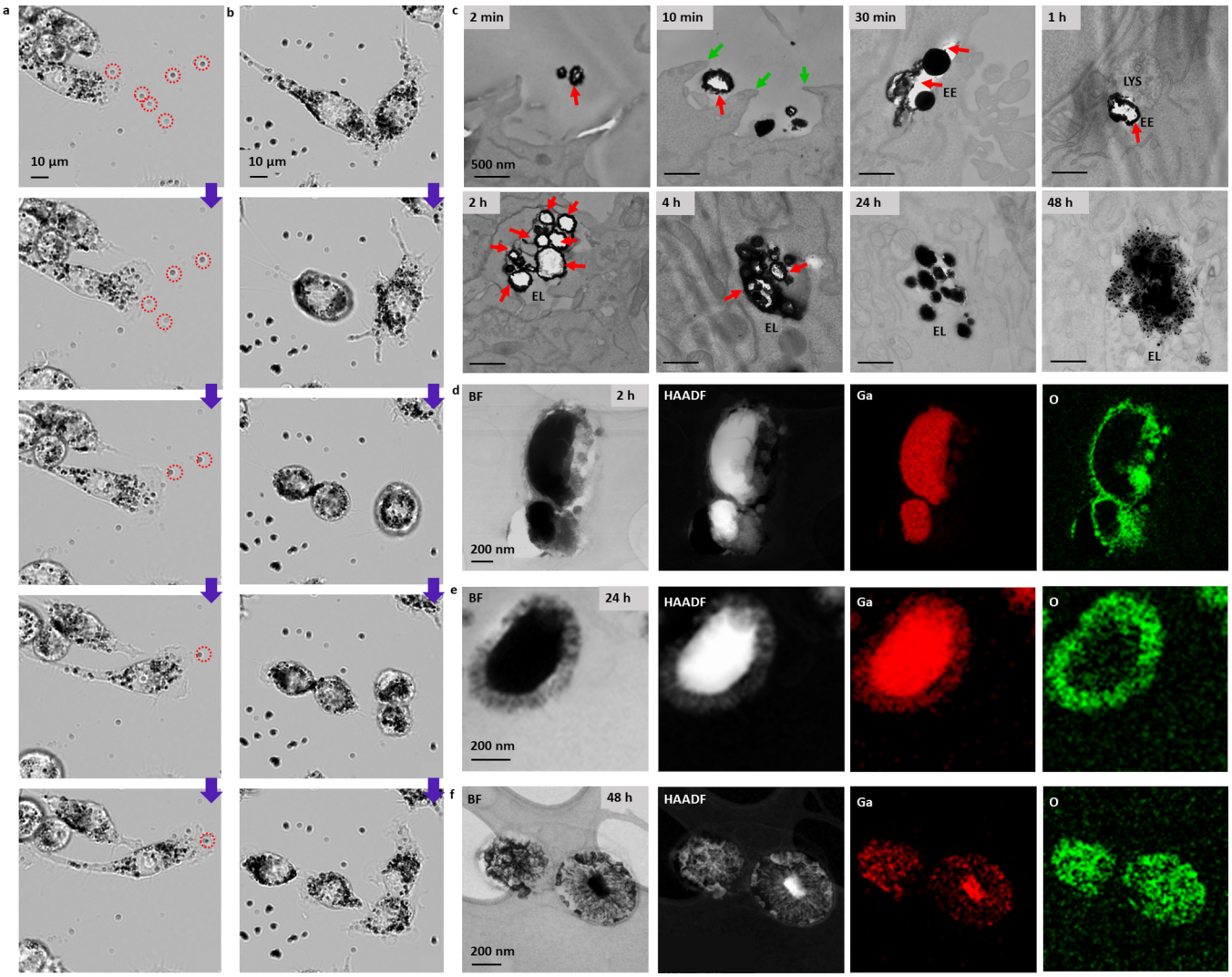

Figure 2. Endocytosis and degradation process of GNDs in RAW 264.7 cells. (a) Representative time-lapse microscopy images (the time sequence is marked by purple arrows) show the process of RAW 264.7 cells endocytosing GNDs. The exampled GNDs were circled with red dotted circles. The individual GNDs (around 300 nm) are too small under microscopy, so they are seen as small gray dots with circled of light diffraction. (b) Representative time-lapse microscopy images (the time sequence is marked by purple arrows) show RAW 264.7 cells split GNDs into daughter cells during mitosis. (c) Representative ultrathin section images of RAW 264.7 cells observed by TEM. The cells were incubated with GNDs for 2, 10, and 30 min and 1, 2, 4, 24, and 48 h. The phagocytosis is indicated with green arrows. The empty cores of some larger GNDs are indicated with red arrows. EE: endosome. LYS: lysosome. EL: endolysosome. (d–f) Representative bright-field (BF) TEM images, high-angle annular dark-field (HAADF) STEM images and EDS elemental maps of GNDs incubated with RAW 264.7 cells for 2 h (d), 24 h (e), and 48 h (f).

The measurements of the released Ga^{3+} (Figure S1) indicate the Ga^{3+} released from the initial Ga bulk and afterward during sonication and also from the synthesized GNDs during storage, are negligible, when EtOH is used as the medium.

Biocompatibility Assessment of GNDs in RAW 264.7 Cells. We chose RAW 264.7 cells, the murine macrophage cell line, as a model cell system that has been suggested to closely mimic inflammatory processes in humans.[38] Because the GNDs were stored in EtOH, to avoid biological contamination and formation of thick oxide layers (which is the case for aqueous solutions), the cytotoxicity of trace EtOH on the RAW 264.7 cells was assessed first (Figure S2 and Supplementary Discussion 1). Then the cytotoxicity of GNDs in the cells was measured with rigorous control of trace EtOH in culture medium below 0.5% (v/v). According to Figure 1e–g, GNDs showed no significant cytotoxicity at 24 and 48 h of up to 2334 μM Ga, and different dimensions showed no significant effect on the RAW 264.7 cell viability. The GNDs at 40 min of sonication (circled with a dotted red box in Figure 1c) were chosen for the later experiments because of the more homogeneous size distribution. Biocompatibility of the GNDs up to 2334 μM with RAW 264.7 cells was further confirmed by live and dead cells assessments (Figure 1h and Figure S3). Compared with results for the control groups at 24 and 48 h, there is no significant increase in dead cells presented in GNDs groups up to 2334 μM of GNDs. The SEM images (Figure 1i and Figure S4) show no significant shape change on the cell morphologies and no visible damage on the cells membrane after GNDs incubation, compared with the control group results.

The transmission electron microscopy (TEM) images in Figure S5 visualized the ultrastructural features of the cells. Compared to the control group, the cells treated with 2334 μM GNDs for 48 h showed similar elongated and cristae-rich

https://doi.org/10.1021/acsnano.1c10981
ACS Nano XXXX, XXX, XXX–XXX

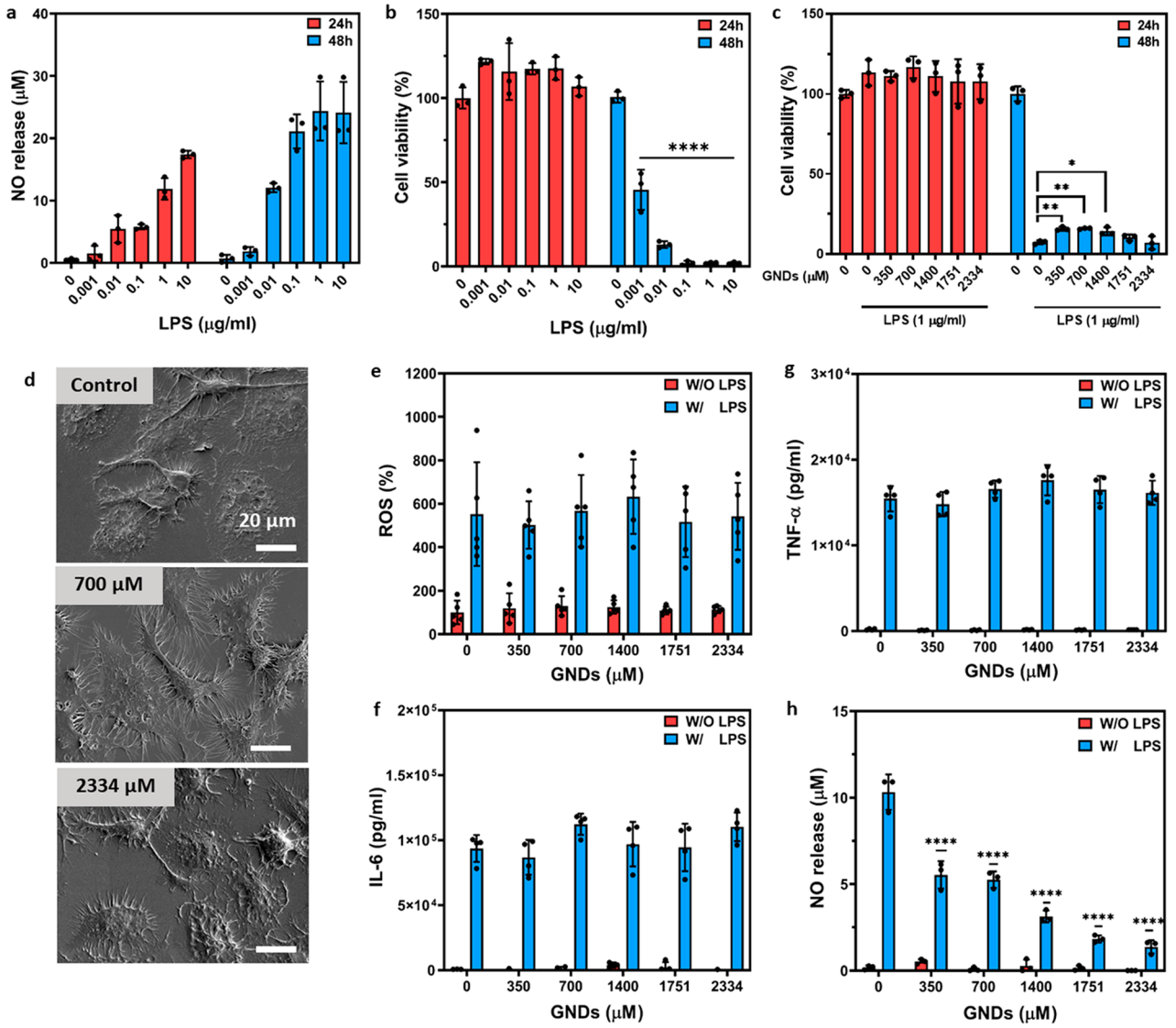

Figure 3. Lipopolysaccharide-induced inflammatory response of RAW 264.7 cells. (a,b) Concentrations of NO released from RAW 264.7 cells (a) and the cell viability of RAW 264.7 cells (b) exposed to different concentrations of LPS at 24 and 48 h. Error bars represent s.d. of n = 3 replicates. (c) Cell viability of RAW 264.7 cells exposed to different concentrations of GNDs with or without the induction of 1 μg mL^{-1} LPS at 24 and 48 h. Error bars represent s.d. of n = 3 replicates. (d) Representative SEM images of RAW 264.7 cells exposed to different concentrations of GNDs with the induction of 1 μg mL^{-1} LPS for 24 h. (e−h) Assessment of the accumulation of ROS (e), IL-6 (f), TNF-α (g), and NO (h) in RAW 264.7 cells, treated with different concentrations of GNDs for 24 h, with or without the induction of 1 μg mL^{-1} LPS. Error bars represent s.d. of n = 5, 4, 4, 3 replicates, respectively. $P < 0.05$ is considered as statistically significant. *$P < 0.05$, **$P < 0.01$, ***$P < 0.001$, and ****$P < 0.0001$.

mitochondria, normal endoplasmic reticulum morphology, and an organelle-rich cytoplasm, which are all indicative of normal viable cells. Altogether, the aforementioned results provide evidence that GNDs have excellent biocompatibility with RAW 264.7 cells when the concentration is kept below 2334 μM. We compared the biocompatibility of cells exposed to GNDs with that of cells exposed to the same concentration of Ga^{3+} (source from $Ga(NO_3)_3$). The GNDs showed better biocompatibility than Ga^{3+}, which presented overt cytotoxicity in RAW 264.7 cells for concentrations above 525 μM in our work (Figure S6) and from 700 μM in a previous report.[1] The cytotoxicity of Ga^{3+} may be contributed by changing the pH of the cell culture medium, generating protein precipitation, which is not seen in GNDs groups (Figure S7).

Assessment of the Endocytosis of GNDs in RAW 264.7 Cells. First, the successful endocytose of GNDs in RAW 264.7 cells were visualized by high-resolution illumination microscopy. The individual GNDs were seen to be easily endocytosed by the RAW 264.7 cells when they were close to the phagocytic tentacles (Figure 2a and Supplementary Video 1), the cells could keep the GNDs internalized for at least 48 h (Supplementary Video 2) and could split GNDs across daughter cells during mitosis (Figure 2b and Supplementary Video 3). The TEM images were employed to confirm the internalization process of the GNDs into RAW 264.7 cells and to determine the ultrastructural machinery responsible for the uptake. As seen in TEM images in Figure 2c, the GNDs were endocytosed by the cells via the process of phagocytosis at the incubation time of 10 min and remained in a single membrane-bound organelle, the endosome. The endosome containing GNDs subsequently fused with lysosome to generate

https://doi.org/10.1021/acsnano.1c10981
ACS Nano XXXX, XXX, XXX−XXX

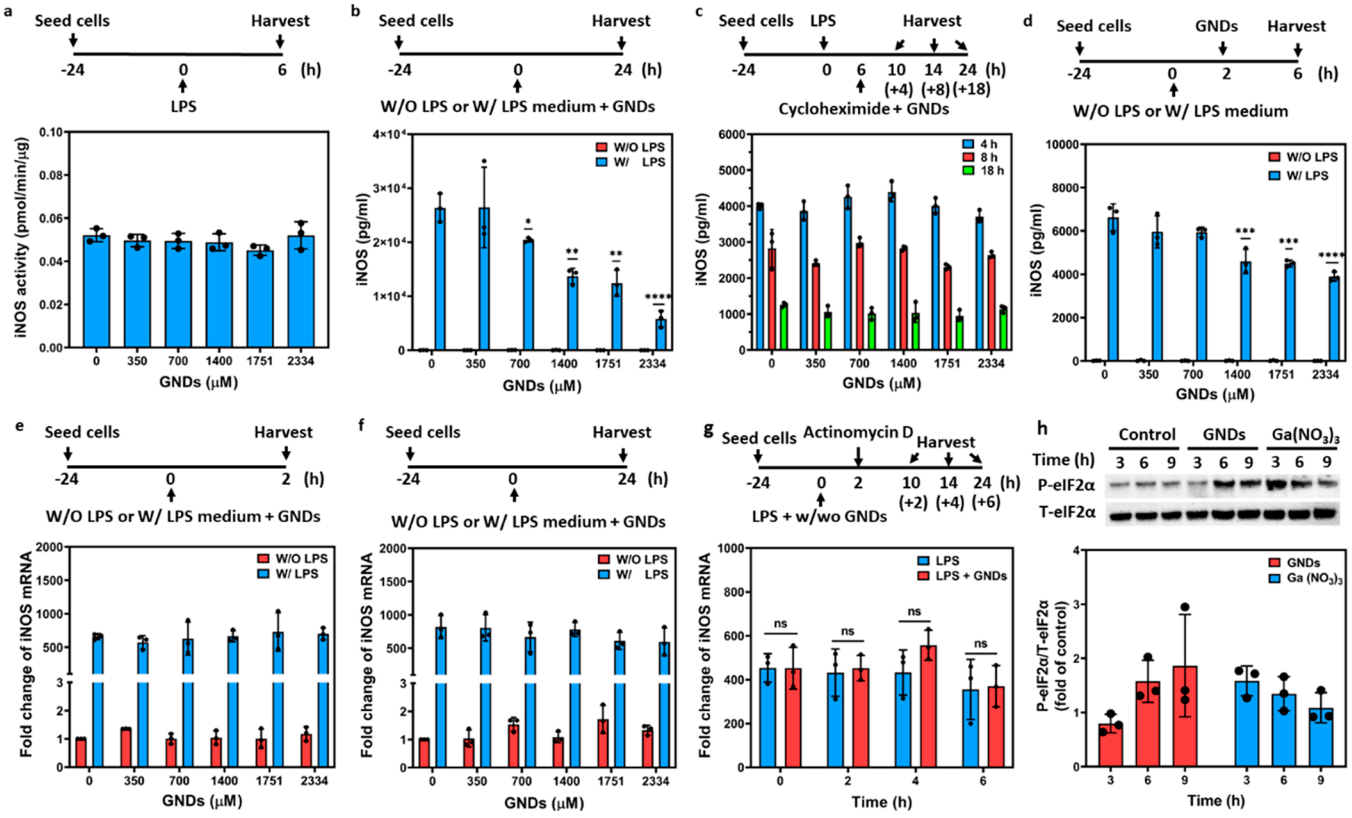

Figure 4. Mechanisms of the inhibitory effect of GNDs on NO release from RAW 264.7 cells. (a) Assessment of enzyme activity of iNOS protein. The cells were induced with 1 μg mL^{-1} LPS for 6 h and harvested for enzyme activity measurement. (b) Assessment of iNOS protein levels in RAW 264.7 cells treated with GNDs for 24 h. The cells were cultured with GNDs for 24 h, with or without the induction of 1 μg mL^{-1} LPS and harvested for measurement. (c) Assessment of the effect of GNDs on iNOS protein stability. The cells were induced with 1 μg m^{-1} LPS for 6 h then treated with GNDs (added with cycloheximide) for 4, 8, and 18 h and harvested for iNOS protein concentrations measurement. (d) Assessment of iNOS protein levels in RAW 264.7 cells treated with GNDs for 4 h. The cells were induced with 1 μg mL^{-1} LPS (or without LPS as control) for 2 h, and GNDs were added for another 4 h and harvested for measurements. (e,f) Assessment of the iNOS gene expression in mRNA level by real-time qRT-PCR. The cells were treated with GNDs with 1 μg mL^{-1} LPS (or without LPS as control) for 2 h (e) or 24 h (f). (g) Assessment of iNOS mRNA stability. The cells were pretreated with 1 μg mL^{-1} LPS with or without GNDs for 2 h. Thereafter, the medium was removed and replaced by the fresh medium containing 5 μg mL^{-1} actinomycin D for 0, 2, 4, and 6 h, respectively. (h) Representative Western blots using antibodies for P-eIF2α (on Ser51) and total eIF2α (T-eIF2α) in LPS-induced RAW 264.7 cells. The cells were treated with 1751 μM GNDs or Ga$(NO_3)_3$ for 3, 6, and 9 h, with the induction of 1 μg mL^{-1} LPS. The levels of eIF2α phosphorylation in Ga-treated groups are normalized with reference to controls which are LPS-treated only. Error bars represent s.d. of n = 3 replicates. P < 0.05 is considered as statistically significant. *P < 0.05, **P < 0.01, ***P < 0.001, and ****P < 0.0001.

endolysosome, a major site of degradation in the cytoplasm,[39] from the time of 1 h.

The empty core of some GNDs shown in those images is because of their liquid property, which could leak out while the cells are sectioned during the specimen preparation. Fewer empty cores were seen with increasing incubation time, which indicates GNDs were gradually transformed from a liquid to a solid state. In combination with thicker Ga oxide layers and more Ga oxides shown in the energy dispersive spectroscopy (EDS) mapping images from time points of 2 h (Figure 2d) to 24 (Figure 2e) and 48 h (Figure 2f), we assume GNDs experienced an oxidative degradation process in the endolysosomes.

Lipopolysaccharide-Induced Inflammatory Response of RAW 264.7 Cells. Lipopolysaccharide, one of the main components on the surface of Gram-negative bacteria, can bind to the Toll-like receptor 4 (TLR4) on the surface of the macrophage and activate the NF-κB signaling pathway to promote inflammation.[40] Inflammation is a natural process of the innate immune system, accompanied by a series of elevated pro-inflammatory mediators, including reactive oxygen species (ROS), pro-inflammatory cytokines (IL-6, TNF-α, and IFN-γ, etc.), and main signaling molecules between immune cells including NO,[41] as illustrated in Figure S8. Guided by previous works[42−44] and the effects of different concentrations of LPS on the NO production from RAW 264.7 cells (Figure 3a), 1 μg mL^{-1} of LPS was chosen to induce the inflammatory response by the cells in this work. The cell viability assessment (Figure 3b) shows LPS from 1 ng mL^{-1} to 10 μg mL^{-1} did not result in significant cytotoxicity up to 24 h, but drastically decreased the cell viability when the incubation time was extended to 48 h even for the lowest concentration (1 ng mL^{-1}). Therefore, in further studies using 1 μg mL^{-1} LPS-induced inflammatory response, experiments were only conducted up to 24 h to avoid confounding signals associated with cell death. Cell viability assessment (Figure 3c and Figure S9) and morphology check (Figure 3d and Figure S10) showed GNDs within the previous screened concentrations (up to 2334 μM) did not bring additional cytotoxicity to inflammatory RAW 264.7 cells (detailed discussed in Supplementary Discussion 2).

To determine the effects of GNDs in LPS-induced inflammatory RAW 264.7 cells, a series of pro-inflammatory

https://doi.org/10.1021/acsnano.1c10981
ACS Nano XXXX, XXX, XXX−XXX

mediators were measured. As shown in Figure 3e−h, the resting RAW 264.7 cells did not illustrate significant accumulation of ROS, IL-6, TNF-α, and NO, whereas those mediators drastically elevated when activated with LPS, which is consistent with the macrophage response to LPS stimulation.[42,44] The treatment of GNDs (up to 2334 μM) in the resting RAW 264.7 cells did not result in a significant effect on those pro-inflammatory mediators, which indicates GNDs do not induce an inflammatory response in the cells. In the LPS-induced inflammatory RAW 264.7 cells, GNDs treatment did not show a considerable effect on the accumulation of ROS, IL-6, and TNF-α in the RAW 264.7 cells, either. Interestingly, GNDs showed a dose-dependent inhibitory effect on NO release from the activated cells. By extension of the incubation time to 48 h (Figure S11), GNDs presented a similar inhibitory trend on the NO release, although the cells started to die after 24 h treatment of the LPS.

Mechanisms of the GNDs Inhibitory Effect on NO Release from LPS-Induced RAW 264.7 Cells. To explore the mechanisms of the inhibitory effect of GNDs on the NO release from RAW 264.7 cells, the iNOS activity and expression, which are responsible for modulating NO during inflammation, were subsequently studied. According to the LPS-induced iNOS signaling pathway illustrated in Figure S12, LPS activates the iNOS gene to induce the iNOS mRNA expression within 2 h and protein expression within 6 h.[30,45,46] The iNOS protein thereafter catalyzes L-arginine to L-citrulline and release NO.[31]

The enzyme activity of iNOS protein was first assessed to determine whether the GNDs inhibitory effect on NO was because of the direct influence on the iNOS catalytic activity. As can be seen in Figure 4a, there was no significant decrease in iNOS activity when exposed to GNDs of any concentration. This result confirms that GNDs do not inhibit the NO release from the LPS-induced RAW 264.7 cells by directly affecting the enzyme activity of iNOS protein.

Gallium ions (sourced from $GaCl_3$ to avoid the interference of NO_3^- from $Ga(NO_3)_3$ in this measurement) were used for comparison and showed a significant inhibitory effect on the enzyme activity of iNOS protein (Figure S13). This result highlights the stark difference of NO release inhibition mechanisms between GNDs and Ga^{3+}.

Having demonstrated no effect on iNOS enzyme activity, we next sought to determine if the GNDs inhibitory effect on NO was on account of inhibition of iNOS protein expression in the LPS-induced RAW 264.7 cells. The iNOS protein expression and its dose response to GNDs are presented in Figure 4b and Figure S14 for 24 and 48 h, respectively. The resting cells did not express the detectable level of iNOS protein, whereas this level drastically increased when the cells were induced by LPS. In the activated cells, the treatment of GNDs for both 24 and 48 h showed a dose-dependent inhibitory effect on the expressions of iNOS protein, although some cells were dead after the LPS induction for 48 h. This result suggests that GNDs regulate iNOS expression under inflammatory conditions, thereby leading to a dose-dependent inhibitory effect on the NO production.

Protein expression can be regulated both by downstream protein degradation and by upstream protein transcription and synthetic processes. To determine whether the NO inhibitory effect of GNDs was because of accelerating the degradation of iNOS protein, the cells with expressed iNOS protein were treated with GNDs (cycloheximide was applied to interrupt further protein synthesis) and the concentrations of the protein at different time points were measured and shown in Figure 4c. The GNDs treatment did not result in a significant decrease in the concentration of iNOS protein within those time durations. Those results suggest that the decreased iNOS expression in the LPS-induced RAW 264.7 cells after GNDs treatment (Figure 4b) was not because of GNDs accelerating iNOS protein degradation.

After the effect on accelerating iNOS protein degradation was eliminated, the effect of GNDs on the iNOS protein synthetic process in the LPS-induced RAW 264.7 cells was assessed. According to the LPS-induced iNOS pathway (Figure S12), LPS can induce the iNOS mRNA expression and protein synthesis process, which have been suggested to take place within 2 and 6 h, respectively.[30,45,46] Therefore, RAW 264.7 cells were induced with LPS for 2 h to ensure the iNOS mRNA expression; then GNDs were added to coincide with the iNOS protein synthesis process and then the freshly expressed proteins were quantified (Figure 4d). In this case, GNDs also showed a dose-dependent inhibitory effect on the iNOS protein expression in the activated cells, which is consistent with the trend illustrated in Figure 4b. Considering the outcomes together (Figure 4a−d), we concluded that the inhibitory effect of GNDs on NO release from the LPS-induced RAW 264.7 cells is on account of perturbing iNOS protein synthesis.

To determine whether the effect on iNOS protein synthesis was because of the suppression of the iNOS gene transcription in LPS-induced RAW 264.7 cells, the iNOS mRNA expression levels were subsequently assessed. The fold changes of iNOS mRNA expression relative to control, in the presence or absence of LPS, with or without the GNDs treatment for 2 and 24 h, were measured. The treatment time of 2 h was chosen according to the LPS-induced iNOS pathway (Figure S12), when the iNOS gene transcription was just completed. The treatment time of 24 h was chosen in relation to the measurement of NO release (Figure 3h) and iNOS protein expression (Figure 4b). As shown in Figure 4e,f, in the resting RAW 264.7 cells, the iNOS mRNA expression was very low and the treatment of GNDs did not induce an increase of the expression of iNOS mRNA. In the activated cells, the expression of mRNA drastically increased; however, GNDs did not lead to any significant inhibitory effect on the iNOS mRNA expression, which is uncorrelated to the iNOS protein expression level shown in Figure 4b,d. The iNOS mRNA stability test (Figure 4g) shows that there was no significant difference in iNOS mRNA stability between LPS-treated only and LPS plus GNDs-treated cells, suggesting that GNDs did not affect the stability of iNOS mRNA. Those results implicated that GNDs interfered with the post-transcriptional regulation of iNOS levels, directly preceding or during translation.

Previous reports in the literature have shown that the increase of the phosphorylation of eukaryotic translation initiation factor (eIF2α) can result in the decrease of iNOS mRNA translation.[47] Additionally, Ga complexes have been reported to increase the phosphorylation of eIF2α.[48] Therefore, we investigated the possible signaling pathway related to the effect of GNDs on the iNOS mRNA translation that may involve eIF2α phosphorylation. We used Western blot analysis to assess the levels of eIF2α phosphorylation by measuring the ratios of phosphorylated eIF2α (P-eIF2α) to total eIF2α (T-

https://doi.org/10.1021/acsnano.1c10981
ACS Nano XXXX, XXX, XXX−XXX

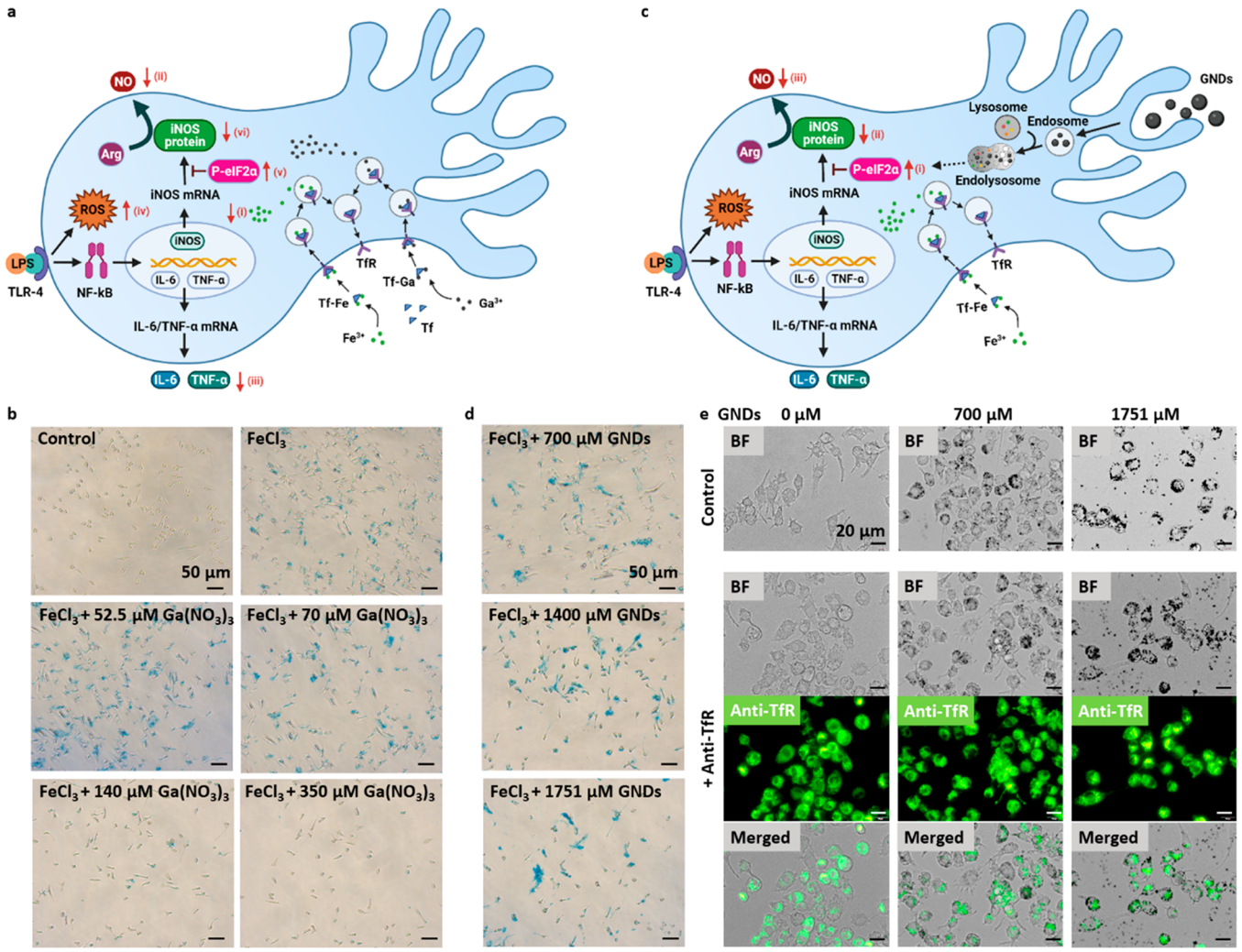

Figure 5. Comparison between GNDs and Ga^{3+} anti-inflammatory effects in LPS-induced RAW 264.7 cells. (a) Ga^{3+} treatment in LPS-induced RAW 264.7 cells. The Ga^{3+} can bind with transferrin (Tf) and be transported into the cells through the TfR-mediated pathway. The competing role of Ga^{3+} with Fe^{3+} in the uptake process leads to the cellular Fe deficiency (pointed with red arrow i), which leads to the reduced release of NO (red arrow ii) and IL-6 and TNF-α (red arrow iii) and the increase of the intracellular ROS (red arrow iv). The Ga^{3+} and the Fe deficiency are proposed to contribute together to upregulate the levels of eIF2α phosphorylation (red arrow v), which results in the reduced iNOS protein expression (red arrow vi) and ultimately NO release (red arrow ii). (b) Prussian blue staining of the cellular Fe^{3+} in RAW 264.7 cells when incubated with different concentrations of $Ga(NO_3)_3$. The concentration of $FeCl_3$: 700 μM. (c) GNDs' treatment in LPS-induced RAW 264.7 cells. GNDs can be endocytosed and remain in the endosomes. When lysosome fuses with endosome, GNDs upregulate the levels of eIF2α phosphorylation (red arrow i) to interfere with the iNOS mRNA translation, which results in the reduced iNOS protein expression (pointed with red arrow ii) and can further inhibit the synthesis of NO from L-arginine (Arg) (pointed with red arrow iii). (d) Prussian blue staining of the cellular Fe^{3+} in RAW 264.7 cells when incubated with different concentrations of GNDs. The concentration of $FeCl_3$: 700 μM. (e) Assessment of the uptake of different concentrations of GNDs (700 and 2334 μM) in LPS-induced RAW 264.7 cells, with or without blocking the TfR by TfR antibodies.

eIF2α) in LPS-induced RAW 264.7 cells, which were treated with various concentrations of GNDs at different times (Figure S15). The result shows the ratio of P-eIF2α to T-eIF2α (P-eIF2α/T-eIF2α) significantly increased when the cells were treated with GNDs from 3 to 9 h. Hence, a higher concentration of GNDs is correlated with the increased levels of eIF2α phosphorylation, which indicates our hypothesis is valid. Because the eIF2α phosphorylation is sometimes related to the response of cellular stress,[49] the P-eIF2α/T-eIF2α in the cells treated with LPS alone were used as the control for normalization. The results presented in Figure 4h show the levels of eIF2α phosphorylation significantly increased when the cells were treated with GNDs for 6 and 9 h, whereas there is no considerable change when the cells were treated for 3 h. A test using Ga^{3+} sourced from $Ga(NO_3)_3$ with the same GNDs concentration was used for comparison. Compared to the Ga^{3+} case, GNDs showed a smaller rate for upregulating the levels of eIF2α phosphorylation, which may be because of the necessary endosomal escape process for GNDs that is not needed for Ga^{3+}. It is interesting to see the levels of eIF2α phosphorylation decreased when the incubation time increased from 3 to 9 h, which indicates the effects of Ga on eIF2α phosphorylation may not be lasting.

To understand the selective inhibitory effect of GNDs on NO, without affecting the pro-inflammatory cytokines, we compared Ga^{3+} with GNDs regarding their anti-inflammatory effects and mechanisms. For Ga^{3+} on an anti-inflammatory in the LPS-induced RAW 264.7 cells (Figure 5a), they can reduce

https://doi.org/10.1021/acsnano.1c10981
ACS Nano XXXX, XXX, XXX−XXX

the release of both NO (Figure S16 and a previous study[1]) and pro-inflammatory cytokines (IL-6, TNF-α[1,4]). Apart from this, Ga^{3+} ions were shown to increase the intracellular ROS levels,[50,51] and it is also proven in this study (Figure S17) when the RAW 264.7 cells were treated with low concentrations ($\leq$140 μM) of Ga^{3+}. The intracellular ROS levels gradually decreased when the concentrations of Ga^{3+} are higher than 175.1 μM, which can be explained by the increased cytotoxicity of Ga^{3+} in those concentrations (Figure S6). The proposed mechanisms of Ga^{3+} on the anti-inflammatory are mainly based on the similarities between Ga^{3+} and Fe^{3+}. Because of the similarities, Ga^{3+} is suggested to bind with transferrin and is transported into the cells through a TfR-mediated pathway.[52,53] The competing role of Ga^{3+} with Fe^{3+} in the uptake process leads to cellular Fe deficiency, which can initiate an influence on both the cell metabolism and global proteins synthesis.[5] This is consistent with our study presented in Figure 5b that describes a decreased uptake of Fe^{3+} by the cells when they are incubated with increased concentrations of Ga^{3+}. The effect of Ga^{3+} on downregulating the expression of iNOS protein (Figure S18) can be explained by the combination of the cellular Fe deficiency[49] and upregulating the levels of P-eIF2α.

For GNDs (Figure 5c), we proved their insignificant effect on the cellular uptake of Fe^{3+} (Figure 5d), which indicates no influence on the Fe homeostasis. The difference of performance between GNDs and Ga^{3+} on the Fe homeostasis can be explained by their different routes of intracellular transmission: TfR-dependent delivery of Ga^{3+} and the TfR-independent delivery of GNDs. The TfR-independent delivery of GNDs is proven in Figure 5e and Figure S19 as there is no significant influence on the uptake of GNDs after blocking the TfR on the RAW 264.7 cells by TfR antibodies, regardless of the presence of LPS. We speculate the direct delivery of GNDs by the cells and consequently the engulfed GNDs locally interfere with iNOS mRNA translation by upregulating the levels of eIF2α phosphorylation, which ultimately results in the selective inhibition of NO release (we proved GNDs have to be internalized to be functional and the results and discussions are presented in Figures S20–S23 and Supplementary Discussion 3). It may sound contradictory that regulating a general translational factor can affect specific mRNAs, actually progressively more evidence has recently shown that eIF2α phosphorylation does not correlate with the global downregulation of protein translation.[49,54] In fact, only lasting and high levels of eIF2α phosphorylation can affect the translation of protein globally, whereas low and middle levels of eIF2α phosphorylation result in the translational control of specific mRNAs.[49] This can be explained by the possibility that weaker mRNAs are easier to be perturbed by small changes in translational factors.[55] In our case, we believe that the iNOS mRNAs tend to be more easily affected by eIF2α phosphorylation than the mRNAs of cytokines, which contributes to the selectivity inhibition of GNDs on NO without affecting cytokines. Therefore, we think the specificity of GNDs on inhibiting NO without affecting pro-inflammatory cytokines can be explained by the observation that (1) GNDs do not affect the Fe homeostasis and (2) GNDs show a selective translational control of iNOS mRNAs by upregulating the levels of eIF2α phosphorylation.

This performance and related mechanisms of GNDs presents the possibility of the superior strategy of using GNDs in comparison to Ga^{3+} for their anti-inflammatory effect because of the following reasons. First, GNDs offer a selective anti-inflammatory effect focusing on NO inhibition without interfering with Fe uptake, unlike Ga^{3+}. This is important as Fe is an essential growth factor for the proliferation and differentiation of all cells, and as such, the use of Ga^{3+} may disrupt Fe homeostasis in untargeted cells, which therefore renders adverse downstream effects on certain Fe-dependent processes.[5] Second, GND treatment contributes to an improvement in biocompatibility compared to treatment with Ga^{3+}, which we speculate is because of the lack of inappropriate Fe^{3+}-mimicry with GNDs and less influence on changing the pH of cell culture medium and protein precipitation. Because biocompatibility is maintained, and NO production is modulated independent of Fe-mediated processes, GNDs have the potential to provide a nuanced control over NO activity through this mechanism.

As for the anti-inflammatory effects of other metal or metal oxide NPs, such as gold,[56] silver,[57,58] and zinc oxide,[59] the general anti-inflammatory effects of these NPs are related to suppressing the extracellular ROS, pro-inflammatory cytokines, and NO production. The mechanisms associated with those affects are based on inhibiting the NF-κB and COX-2 pathways, or modulating MAPK and PI3K pathways, and suppressing the iNOS expression. Compared to those metal or metal oxide NPs, GNDs show a fairly selective anti-inflammatory effect only on modulating NO production, and the mechanism is based on inhibiting iNOS expression by interrupting the iNOS mRNA translation process.

CONCLUSIONS

We synthesized and characterized GNDs, low-dimensional Ga in a liquid state, and proved the successful uptake and transport of GNDs by RAW 264.7 cells. The interaction of GNDs with RAW 264.7 cells was studied to obtain the cytotoxicity concentration threshold for GNDs, which was thereafter used as guidance to maintain the cell viability across the experimental concentrations. For assessing the anti-inflammatory effects of GNDs in LPS-induced RAW 264.7 cells, the accumulation of pro-inflammatory mediators was measured. The GNDs did not reveal any significant influence on the accumulation of pro-inflammatory mediators while showing an inhibitory effect on NO production. To explore the mechanisms of this inhibitory effect, iNOS, which is responsible for releasing NO during inflammation, was subsequently studied. We confirmed that GNDs inhibited the NO production because of reducing the expression of iNOS protein, without affecting the enzyme activity and stability of iNOS protein and the expression and stability of iNOS mRNA. Therefore, we concluded that GNDs are most likely to inhibit the iNOS mRNA translation to iNOS protein by upregulating the levels of eIF2α phosphorylation in LPS-induced RAW 264.7, which revealed an unexpected mechanism in contrast to the classical view of Ga as an anti-inflammatory agent that relies on the Fe-mimicry.

The different performances between those two forms of Ga can be explained by their various routes of intracellular transmission: the TfR-dependent delivery of Ga^{3+} and the direct uptake of GNDs. Those different mechanisms reveal GNDs' overall superiority in comparison to that of Ga^{3+} for the anti-inflammatory effect because of its selectivity on inhibiting NO production without affecting the Fe^{3+} TfR-mediated endocytosis and further Fe homeostasis. The lack of inappropriate Fe^{3+} mimicry with GNDs also contributes to

https://doi.org/10.1021/acsnano.1c10981
ACS Nano XXXX, XXX, XXX−XXX

an improvement in biocompatibility compared to that with Ga^{3+}. Furthermore, the direct transport of Ga into macrophages through nanodroplets provides an avenue to probe intracellular roles of Ga beyond Fe-mimicry, something that was not possible with conventional Ga^{3+} based compounds.

This work fills the knowledge gap of understanding Ga functionality in the liquid metal state as an anti-inflammatory agent and compares the functionality of GNDs with the conventional use of Ga in the form of ions. This understanding and the comparison with Ga ions reveal molecular basis of GND−macrophage interactions that provides a guide for future investigations and offers a base for innovative use of Ga as an anti-inflammatory agent and the implementation of GNDs in biomedical and pharmaceutical applications. In addition to this, GNDs are liquid at physiological temperatures and represent highly transformable and stimuli-responsive entities, which make them specifically appealing for *in vivo* applications, where targeted delivery, release of drugs, and other direct effects within cells and organelles can be harnessed for treatment.

METHODS AND MATERIALS

Preparation of Gallium Nanodroplets. The synthesis of the GNDs was conducted in one direct step. In a typical experiment, 1.1 g of Ga (round shots of 2.0−3.0 mm, 99.999% purity, RotoMetals Inc., USA) was added into 10 mL of EtOH (100%, undenatured, Chem-Supply, Australia) in a 25 mL glass vial. The glass vial was then put inside a 40 °C water bath until Ga was melted and sonicated by a probe sonicator (SONICS VCX 750, Amp: 40%) in burst mode (on/off: 9/1s). Gallium was sonicated for the duration of 10, 20, 30, 40, and 50 min and the samples were stored in EtOH for use. To measure the concentrations of produced GNDs, specific amounts of GNDs were fully dissolved in 1 M hydrogen chloride (HCl), and then the concentrations of Ga element were assessed using an inductively coupled plasma (ICP-OES, PerkinElmer, USA) process.

Morphological Analyses of Gallium Nanodroplets. The morphologies of the synthesized GNDs were characterized by SEM (JEOL JSM-IT 500 HR, Japan). The SEM samples were obtained by drop-casting 10 μL of GNDs suspensions onto silicon wafers.

Cell Culture for RAW 264.7 Cells. Murine macrophage cells, RAW 264.7 cell line (originally purchased from American Type Culture Collection, USA), were cultured in Dulbecco's modified eagle's medium (DMEM, low glucose, Cat. No. 11885084, Sigma-Aldrich, Australia) and supplemented with 10% fetal bovine serum (FBS, Australia origin, Cat. No. 12003C, Sigma-Aldrich, Australia) and 5 mL of L-glutamine solution (200 mM, Cat. No. G7513, Sigma-Aldrich, Australia) at 37 °C in an incubator containing 5% CO_2. The medium was changed every 2 days during incubation or subcultured for experiments when confluence is reached. Lipopolysaccharide (LPS, from *Escherichia coli* O127:B8, Cat. No. L4516, Sigma-Aldrich, Australia) was used in this work to induce inflammatory response in RAW 264.7 cells. The passage of RAW 264.7 cell line used in this work was controlled between 19 and 30.

Cell Viability/Metabolic Activity. The cell viability/metabolic activity of RAW 264.7 cells was determined by Cell Counting Kit 8 (CCK8, Cat. No. ab228554, Abcam, UK). In a typical procedure, RAW 264.7 cells (10^4/well) were first seeded in 96-well plates. After 24 h, cells were treated with different concentrations of experimental groups for 24 and 48 h. In separate experiments in this work, experimental groups were different concentrations of EtOH, GNDs and $Ga(NO_3)_3$, respectively. After the specific treatments, the old medium was replaced by a premixed fresh medium containing 10% of CCK8 and incubated for another 90 min. To avoid the inherent absorbance of cells and samples, the supernatant was transferred to a new 96-well plate and absorbance at 460 nm was monitored using a microplate reader (Clariostar Plus, BMG Labtech). To assess whether the samples by themselves could interfere with the measurements, a group of GNDs without cells were used at the same time as controls.

Live and Dead Cells Assessment. Live and dead cells were studied with the Live/Dead Cell Double Staining Kit (Cat. No. 04511, Sigma-Aldrich, Australia). In a typical procedure, RAW 264.7 cells (10^5/well) were first seeded in 12-well plates. After 24 h, cells were treated with different concentrations of experimental groups for 24 and 48 h, respectively. After the treatment, the cells were collected and incubated with a mixture of calcein-AM (2 μM) and propidium iodide (PI) (1.5 μM) according to the standard protocol recommended by the kit and captured by a fluorescent microscope (Olympus IX73, Japan).

Morphological Analyses of RAW 264.7 Cells Endocytosed with Gallium Nanodroplets. To characterize the morphologies of RAW 264.7 cells, when endocytosed with GNDs, cells were fixed overnight at 4 °C using a 2.5% glutaraldehyde in 0.1 M sodium phosphate buffer after incubated with GNDs for 12, 24, and 48 h. Afterward, the fixed cells were washed using a sodium phosphate buffer and dehydrated by EtOH and hexamethyldisilizane (HMDS) and left to air-dry in a final 100% solution of HMDS. Consequently, samples were coated with a 10 nm platinum layer (Q3000 dual coater, Quorum Tech., UK) and viewed using SEM.

Subcellular Structure Analyses of RAW 264.7 Cells Endocytosed with Gallium Nanodroplets. To characterize the subcellular structures of RAW 264.7 cells, when endocytosed with GNDs, TEM was used. In a typical procedure, the RAW 264.7 cells (10^5/well) were seeded onto round sterile glass coverslips placed inside a 12-well plate for 24 h and treated with 2334 μM GNDs for different time durations (2, 10, and 30 min and 1, 2, 4, 24, and 48 h). After treatment, cells were first fixed by glutaraldehyde; then the samples were dehydrated by EtOH and infiltrated with resin (Procure, 812) following a standard protocol. The samples were cut using a diamond knife (Diatome) into ultrathin sections (the thickness is around 70 nm) and transferred onto carbon-coated copper holey TEM grids and imaged using a JEOL 1400 TEM operating at 100 kV and JEOL F200 TEM (Tokyo, Japan) operating at 200 kV.

High Resolution Live Cell Imaging System. GNDs association with cells were observed under a high-resolution microscopy system (Celldiscoverer 7, Zeiss). RAW 264.7 cells (10^5/well) were seeded in 12-well plates for 24 h and treated with GNDs. Cells were then transferred to the imaging chamber (set the temperature at 37 °C and connected to 5% CO_2), and images were taken at a 4 min sampling rate.

Assessment of Reactive Oxygen Species Production. The generation of intracellular reactive oxygen species (ROS) was assessed using the DCFDA/H2DCFDA−Cellular ROS Assay Kit (Cat. No. ab113851, Abcam, UK). The cell-permeable 2′7′-dichlorodihydrofluorescein (DCF-DA) is oxidized by intracellular reactive oxygen species to the highly fluorescent DCF. In a typical procedure, RAW 264.7 cells (10^4/well) were first seeded in 96-well plates with black wall and clear bottom. After 24 h, cells were treated with different concentrations of experimental groups for 24 and 48 h, respectively. After the treatment, cells were washed with buffer and incubated with 20 μM DCFDA solution for 45 min at 37 °C. After incubation, the fluorescence of cells was read at Ex/Em = 485/535 nm using a microplate reader. To assess whether the samples alone can interfere with the measurement, a group of GNDs without cells were used at the same time as controls.

Assessment of Pro-inflammatory Cytokines Production. The concentrations of pro-inflammatory cytokines IL-6, TNF-α, and IFN-γ were measured by enzyme-linked immunosorbent assay (ELISA) using a Mouse IL-6 ELISA Kit (Cat. No. ab222503, Abcam), a Mouse TNF alpha ELISA Kit (Cat. No. ab208348, Abcam), and a Mouse Interferon gamma ELISA Kit (Cat. No. ab100689, Abcam), respectively. In a typical procedure, RAW 264.7 cells (10^5/well) were seeded in 12-well plates. After 24 h, cells were treated with different concentrations of GNDs with or without LPS (1.0 μg mL^{-1}) for 24 h. The supernatants were collected to measure the concentrations of IL-6, TNF-α, and IFN-γ according to the manufacturer's instructions.

https://doi.org/10.1021/acsnano.1c10981
ACS Nano XXXX, XXX, XXX−XXX

Assessment of Nitric Oxide Production. The generation of NO was determined by detecting the production of nitrite by the Griess reaction[60] with Griess reagent (Cat. No. G4410, Sigma-Aldrich, Australia). In a typical procedure, RAW 264.7 cells (10^4/well) were seeded in 96-well plates. After 24 h, cells were then treated with different concentrations of experimental groups for 24 and 48 h. After treatment, the supernatants were transferred to a new 96-well plate and mixed with equal volumes of Griess reagent, and then the absorbance was read at 540 nm after 15 min. To assess whether the samples alone could interfere with the measurements, a group of GNDs without cells were used at the same time as controls.

Assessment of the Enzyme Activity of Inducible Nitric Oxide Synthase. The enzyme activity of inducible NO synthase was measured by a Nitric Oxide Synthase Activity Assay Kit (Fluorometric, Cat. No. ab211084, Abcam). In a typical procedure, 3×10^7 RAW 264.7 cells were induced with 1 μg mL^{-1} LPS for 6 h, and then cells were harvested and homogenized to make cell lysate. The whole protein concentration in cell lysate was quantified using a bicinchoninic acid (BCA) assay (Cat. No. QPBCA, QuantiPro BCA Assay Kit, Sigma-Aldrich, Australia). Then the same amount of fresh cell lysate (containing 200 μg protein) was mixed with different concentrations of GNDs (350−2334 μM) and the iNOS activity was measured according to manufacturer's instructions. The mixture of cell lysates and different concentrations of GNDs added with assay buffer were run in parallel as background controls.

The iNOS activity was defined using:

$$\text{iNOS activity} = \left(\frac{B}{T \times C}\right) \quad (1)$$

where:

B = nitrite amount in sample well from the standard curve (pmol)

T = reaction time (minutes)

C = the amount of protein (μg)

Assessment of Inducible Nitric Oxide Synthase Expression. For measuring the effect of GNDs on iNOS expression, RAW 264.7 cells (3×10^5/well) were first seeded in 6-well plates. After 24 h, cells were treated with different concentrations of GNDs (or medium alone as control) with or without LPS (1.0 μg mL^{-1}) for 24 and 48 h, respectively.

For measuring the effect of GNDs on iNOS mRNA translation, RAW 264.7 cells (3×10^5/well) were seeded in 6-well plates and treated with LPS (1.0 μg mL^{-1}) for 2 h. Afterward, the cells were treated with GNDs (or medium alone as control) for another 4 h.

For measuring the effect of GNDs on the iNOS protein stability, RAW 264.7 cells (3×10^5/well) were seeded in 6-well plates and treated with LPS (1.0 μg mL^{-1}) for 6 h. Afterward, the cells were treated with GNDs (or medium alone as control) for another 4, 8, and 18 h, respectively. Cycloheximide (10 μg mL^{-1}) was applied to the medium to interrupt further protein synthesis.

The treated cells mentioned above in each group were harvested and the whole protein was extracted, respectively. The extracted protein was quantified using a bicinchoninic acid (BCA) assay (Cat. No. QPBCA, QuantiPro BCA Assay Kit, Sigma-Aldrich, Australia) and the concentrations of iNOS based on a 60 μg mL^{-1} extract load were measured by Mouse iNOS ELISA Kit (Cat. No. ab253219, Abcam) according to the manufacturer's instructions.

RNA Isolation and mRNA Analysis by Real-Time Quantitative Reverse Transcription Polymerase Chain Reaction. Cells were seeded with the density of 10^5 cells per well in 12-well plates. After 24 h, cells were treated with different concentrations of GNDs with or without LPS (1.0 μg mL^{-1}) for 2 or 24 h. The total RNA was isolated by using a RNeasy Plus Mini Kit (Cat. No. 74136, Qiagen, Germany), and the concentrations were then measured by Nanodrop (Nanodrop One, Thermo Scientific, USA).

The mRNA expression of iNOS was evaluated by quantitative real-time quantitative reverse transcription polymerase chain reaction (Real-Time qRT-PCR) in triplicate, and the mRNA level of β-actin was used as an internal control. The following primers were used: Mouse iNOS, GGCAGCCTGTGAGACCTTTG (sense) and GCATTGGAAGTGAAGCGTTTC (antisense); Mouse β-actin, AGAGGGAAATCGTGCGTGAC (sense) and CAATAGTGATGACCTGGCCGT (antisense).[43] As the template, 200 ng of total RNA from each sample was used. RT-qPCR was performed using the iTaq Universal SYBR Green One-Step Kit (Cat. No. 1725151, Bio-Rad, USA) on a CFX96 Touch Real-Time PCR Detection System (Bio-Rad Laboratories, Inc., USA) following the standard protocol recommended by the kit. The levels of iNOS gene expression were measured by comparative quantification algorithms.[61]

Cellular Uptake of Fe^{3+} Staining. The cellular uptake of Fe^{3+} was assessed by an Iron Stain Kit (Cat. No. ab150674, Abcam, UK) based on Prussian blue. The cells were seeded onto 12 well plates and incubated with $FeCl_3$ and different concentrations of GNDs or $Ga(NO_3)_3$ for 24 h. Then the cellular Fe^{3+} was stained according to the manufacturer's instructions. The images of stained cells were captured using a color camera (Infinity 5-5, Teledyne Lumenera, Canada)-equipped microscope (Olympus CKX53, Japan).

Antibody Blocking and Down-Regulation of TfR. An antimouse TfR monoclonal antibody (FITC Rat Anti-Mouse CD71, Cat. No. 567260, BD Biosciences Pharmingen, USA) was used for blocking and down-regulation of TfR on the RAW 264.7 cells. Cells were preincubated with 5 μg mL^{-1} of the TfR antibodies for 1 h before incubating with different concentrations of GNDs. The images of cells were captured and observed using a camera-equipped fluorescent microscope (Olympus IX73, Japan).

Western Blotting Analysis. The antibodies were acquired from Cell Signaling Technology (Beverly, MA, USA): eIF2α antibody (#9722), Phospho-eIF2α (Ser51) antibody (#9721), antirabbit IgG, HRP-linked antibody (#7074), and β-actin (D6A8) Rabbit mAb (#8457). After different treatments, the RAW 264.7 cells were lysed by RIPA buffer (Cata. No. 89900, Thermo Scientific, USA) added with Halt Phosphatase (Cata. No. 78420, Thermo Scientific, USA) and Protease (Cata. No. ab65621, Abcam, UK) Inhibitor Cocktails. The total protein concentrations were assessed by a bicinchoninic acid assay (Cat. No. QPBCA, QuantiPro BCA Assay Kit, Sigma-Aldrich, Australia), 35−40 μg of protein were loaded for electrophoresis into protein gels (Cata. No. NP0315BOX, Thermo Scientific, USA) and afterward transferred onto PVDF membranes (Cata. No. LC2002, Thermo Scientific, USA). Consequently, the Western blotting substrates (Cata. No. 32109, Thermo Scientific, USA) were added and ChemiDoc Imaging System (Bio-Rad Laboratories, Inc., USA) were used for visualization.

Statistical Analysis. Each experiment was repeated at least three times with each assay in triplicate. Data are expressed as mean ± standard deviation (s.d.). Statistical significance was calculated using one-way ANOVA in Prism 8.0.2 (GraphPad Software Inc.) to compare differences between the treatment groups and control group. $P < 0.05$ is considered as statistically significant. P value style: $^*P < 0.05$, $^{**}P < 0.01$, $^{***}P < 0.001$, and $^{****}P < 0.0001$.

ASSOCIATED CONTENT

Supporting Information

The Supporting Information is available free of charge at https://pubs.acs.org/doi/10.1021/acsnano.1c10981.

Figures S1−23, measurement of the released amounts of Ga ions during sonication and storage in EtOH, cytotoxicity assessment of trace EtOH, representative live and dead double fluorescence staining images of RAW 264.7 cells incubated with GNDs for 24 and 48 h, representative SEM images of RAW 264.7 cells incubated with GNDs for 6 and 24 h, representative TEM images of RAW 264.7 cells incubated with GNDs for 48 h, cytotoxicity assessment of $Ga(NO_3)_3$, photo of different concentrations of GNDs and $Ga(NO_3)_3$ in cell culture medium within 24 h, LPS-induced inflammatory response of RAW 264.7 cells, representative SEM images

https://doi.org/10.1021/acsnano.1c10981
ACS Nano XXXX, XXX, XXX−XXX

for assessing the morphology of macrophages after incubated with GNDs, concentrations of NO released from RAW 264.7 cells, LPS-induced iNOS signaling pathway, assessment of the effects of $GaCl_3$ on the enzyme activity of iNOS protein, assessment of iNOS gene expression in protein level, representative Western blots using antibodies, concentrations of NO released from RAW 264.7 cells incubated with $Ga(NO_3)_3$ for 24 and 48 h, assessment of intracellular ROS levels in RAW 264.7 cells incubated with $Ga(NO_3)_3$ for 24 h, assessment of iNOS protein levels, assessment of GNDs uptake in RAW 264.7 cells, representative SEM images of PEG coated GNDs and micro GDs, observation of the cellular uptake of different particles in RAW 264.7 cells, concentrations of NO production and the cell viability treated by micro GDs, and concentrations of Ga^{3+} released from micro GDs; Table S1, dimensions of GNDs sonicated for different durations; Discussions 1−3, assessment of the cytotoxicity of trace EtOH in RAW 264.7 cells, assessment of the cytotoxicity of GNDs in LPS-induced inflammatory RAW 264.7 cells, and assessment of the functions of micro GDs in LPS-induced inflammatory RAW 264.7 cells (PDF)

Endocytosis process of GNDs in macrophages (MP4)

Endocytosis process of GNDs in macrophages (within 48 h) (MP4)

Macrophages split the GNDs into daughter cells (MP4)

AUTHOR INFORMATION

Corresponding Authors

Dorna Esrafilzadeh − *Graduate School of Biomedical Engineering, University of New South Wales (UNSW), Sydney, NSW 2052, Australia;* orcid.org/0000-0002-2539-294X; Email: d.esrafilzadeh@unsw.edu.au

Kourosh Kalantar-Zadeh − *School of Chemical Engineering, University of New South Wales (UNSW), Sydney, NSW 2052, Australia;* orcid.org/0000-0001-6109-132X; Email: k.kalantar-zadeh@unsw.edu.au

Authors

Chengchen Zhang − *School of Chemical Engineering, University of New South Wales (UNSW), Sydney, NSW 2052, Australia;* orcid.org/0000-0001-8802-539X

Biyao Yang − *ARC Centre of Excellence for Nanoscale BioPhotonics, Graduate School of Biomedical Engineering, University of New South Wales (UNSW), Sydney, NSW 2052, Australia*

Joanna M. Biazik − *Electron Microscope Unit, Mark Wainwright Analytical Centre, University of New South Wales (UNSW), Sydney, NSW 2052, Australia*

Richard F. Webster − *Electron Microscope Unit, Mark Wainwright Analytical Centre, University of New South Wales (UNSW), Sydney, NSW 2052, Australia;* orcid.org/0000-0003-1414-928X

Wanjie Xie − *School of Chemical Engineering, University of New South Wales (UNSW), Sydney, NSW 2052, Australia*

Jianbo Tang − *School of Chemical Engineering, University of New South Wales (UNSW), Sydney, NSW 2052, Australia;* orcid.org/0000-0002-0155-6807

Francois-Marie Allioux − *School of Chemical Engineering, University of New South Wales (UNSW), Sydney, NSW 2052, Australia;* orcid.org/0000-0003-0973-5110

Roozbeh Abbasi − *School of Chemical Engineering, University of New South Wales (UNSW), Sydney, NSW 2052, Australia;* orcid.org/0000-0002-2449-4282

Maedehsadat Mousavi − *School of Chemical Engineering, University of New South Wales (UNSW), Sydney, NSW 2052, Australia;* orcid.org/0000-0003-3403-9133

Ewa M. Goldys − *ARC Centre of Excellence for Nanoscale BioPhotonics, Graduate School of Biomedical Engineering, University of New South Wales (UNSW), Sydney, NSW 2052, Australia*

Kristopher A. Kilian − *School of Chemistry, School of Materials Science and Engineering, Australian Centre for NanoMedicine, University of New South Wales (UNSW), Sydney, NSW 2052, Australia;* orcid.org/0000-0002-8963-9796

Rona Chandrawati − *School of Chemical Engineering, University of New South Wales (UNSW), Sydney, NSW 2052, Australia;* orcid.org/0000-0002-9780-8844

Complete contact information is available at: https://pubs.acs.org/10.1021/acsnano.1c10981

Author Contributions

C.Z. made the preliminary experimental observations. C.Z. and K.K.-Z. conceived and designed the experiments. C.Z. conducted the experiments and characterizations and analyzed the data with the help of B.Y. and J.M.B., J.T., F.-M.A., W.X., R.A., M.M., E.M.G., K.A.K., R.C., R.F.W., and D.E.. The first manuscript was drafted by C.Z. and K.K.-Z. with input from all the authors.

Notes

The authors declare no competing financial interest.

ACKNOWLEDGMENTS

The authors acknowledge the Australian Research Council (ARC) Laureate Fellowship grant (FL180100053) for the financial coverage of this work. The authors thank the Electron Microscope Unit and the Katharina Gaus Light Microscopy Facility within the Mark Wainwright Analytical Centre at UNSW Sydney. The authors also thank Dr. Lin Zhang from the School of Chemistry, UNSW, for donating the RAW 264.7 cells and Dr. Ruirui Qiao from the Australian Institute for Bioengineering and Nanotechnology (The University of Queensland) for donating the functionalized PEG.

REFERENCES

(1) Makkonen, N.; Hirvonen, M.-R.; Savolainen, K.; Lapinjoki, S.; Mönkkönen, J. The Effect of Free Gallium and Gallium in Liposomes on Cytokine and Nitric Oxide Secretion from Macrophage-Like Cells in Vitro. *J. Inflamm. Res.* **1995**, *44* (12), 523−528.

(2) de Albuquerque Wanderley Sales, V.; Timóteo, T. R. R.; da Silva, N. M.; de Melo, C. G.; Ferreira, A. S.; de Oliveira, M. V. G.; de Oliveira Silva, E.; Dos Santos Mendes, L. M.; Rolim, L. A.; Neto, P. J. R. A Systematic Review of the Anti-Inflammatory Effects of Gallium Compounds. *Curr. Med. Chem.* **2021**, *28* (10), 2062−2076.

(3) Matkovic, V.; Balboa, A.; Clinchot, D. M.; Whitacre, C. C.; Zwilling, B. S.; Brown, D.; Weisbrode, S. E.; Apseloff, G.; Gerber, N. Gallium Prevents Adjuvant Arthritis in Rats and Interferes with Macrophage/T-Cell Function in the Immune Response. *Curr. Ther. Res.* **1991**, *50* (2), 255−267.

(4) Bernstein, L. R. Mechanisms of Therapeutic Activity for Gallium. *Pharmacol. Rev.* **1998**, *50* (4), 665−682.

(5) Chitambar, C. R. Gallium and its Competing Roles with Iron in Biological Systems. *Biochim. Biophys. Acta, Mol. Cell Res.* **2016**, *1863* (8), 2044−2053.

(6) Boldt, D. H. New Perspectives on Iron: An Introduction. *Am. J. Med. Sci.* **1999**, *318* (4), 207−212.
(7) Kirtane, A. R.; Verma, M.; Karandikar, P.; Furin, J.; Langer, R.; Traverso, G. Nanotechnology Approaches for Global Infectious Diseases. *Nat. Nanotechnol.* **2021**, *16* (4), 369−384.
(8) Poon, W.; Kingston, B. R.; Ouyang, B.; Ngo, W.; Chan, W. C. W. A Framework for Designing Delivery Systems. *Nat. Nanotechnol.* **2020**, *15* (10), 819−829.
(9) Lu, Y.; Hu, Q.; Lin, Y.; Pacardo, D. B.; Wang, C.; Sun, W.; Ligler, F. S.; Dickey, M. D.; Gu, Z. Transformable Liquid-Metal Nanomedicine. *Nat. Commun.* **2015**, *6* (1), 10066.
(10) Lu, Y.; Lin, Y.; Chen, Z.; Hu, Q.; Liu, Y.; Yu, S.; Gao, W.; Dickey, M. D.; Gu, Z. Enhanced Endosomal Escape by Light-Fueled Liquid-Metal Transformer. *Nano Lett.* **2017**, *17* (4), 2138−2145.
(11) Yan, J.; Lu, Y.; Chen, G.; Yang, M.; Gu, Z. Advances in Liquid Metals for Biomedical Applications. *Chem. Soc. Rev.* **2018**, *47* (8), 2518−2533.
(12) Yu, Y.; Miyako, E. Recent Advances in Liquid Metal Manipulation toward Soft Robotics and Biotechnologies. *Chem.—Eur. J.* **2018**, *24* (38), 9456−9462.
(13) Miyako, E. Convergence of Liquid Metal Biotechnologies for Our Health. *Acc. Mater. Res.* **2021**, *2* (10), 858−862.
(14) Kalantar-Zadeh, K.; Tang, J.; Daeneke, T.; O' Mullane, A. P.; Stewart, L. A.; Liu, J.; Majidi, C.; Ruoff, R. S.; Weiss, P. S.; Dickey, M. D. Emergence of Liquid Metals in Nanotechnology. *ACS Nano* **2019**, *13* (7), 7388−7395.
(15) Cheeseman, S.; Elbourne, A.; Gangadoo, S.; Shaw, Z. L.; Bryant, S. J.; Syed, N.; Dickey, M. D.; Higgins, M. J.; Vasilev, K.; McConville, C. F.; Christofferson, A. J.; Crawford, R. J.; Daeneke, T.; Chapman, J.; Truong, V. K. Interactions between Liquid Metal Droplets and Bacterial, Fungal, and Mammalian Cells. *Adv. Mater. Interfaces* **2022**, *9* (7), 2102113.
(16) Xu, D.; Hu, J.; Pan, X.; Sánchez, S.; Yan, X.; Ma, X. Enzyme-Powered Liquid Metal Nanobots Endowed with Multiple Biomedical Functions. *ACS Nano* **2021**, *15* (7), 11543−11554.
(17) Wang, D.; Gao, C.; Zhou, C.; Lin, Z.; He, Q. Leukocyte Membrane-Coated Liquid Metal Nanoswimmers for Actively Targeted Delivery and Synergistic Chemophotothermal Therapy. *Research* **2020**, *2020*, 3676954.
(18) Liu, Q.; Meng, S.; Zheng, T.; Liu, Y.; Ma, X.; Feng, H. Alkaline-Driven Liquid Metal Janus Micromotor with a Coating Material-Dependent Propulsion Mechanism. *ACS Appl. Mater. Interfaces* **2021**, *13* (30), 35897−35904.
(19) Sun, X.; Yuan, B.; Rao, W.; Liu, J. Amorphous Liquid Metal Electrodes Enabled Conformable Electrochemical Therapy of Tumors. *Biomaterials* **2017**, *146*, 156−167.
(20) Yan, J.; Zhang, X.; Liu, Y.; Ye, Y.; Yu, J.; Chen, Q.; Wang, J.; Zhang, Y.; Hu, Q.; Kang, Y.; Yang, M.; Gu, Z. Shape-Controlled Synthesis of Liquid Metal Nanodroplets for Photothermal Therapy. *Nano Res.* **2019**, *12* (6), 1313−1320.
(21) Wang, D.; Gao, C.; Wang, W.; Sun, M.; Guo, B.; Xie, H.; He, Q. Shape-Transformable, Fusible Rodlike Swimming Liquid Metal Nanomachine. *ACS Nano* **2018**, *12* (10), 10212−10220.
(22) Chechetka, S. A.; Yu, Y.; Zhen, X.; Pramanik, M.; Pu, K.; Miyako, E. Light-Driven Liquid Metal Nanotransformers for Biomedical Theranostics. *Nat. Commun.* **2017**, *8* (1), 15432.
(23) Xia, N.; Li, N.; Rao, W.; Yu, J.; Wu, Q.; Tan, L.; Li, H.; Gou, L.; Liang, P.; Li, L.; Meng, X. Multifunctional and Flexible ZrO_2-Coated EGaIn Nanoparticles for Photothermal Therapy. *Nanoscale* **2019**, *11* (21), 10183−10189.
(24) Huang, Y.; Yang, F.; Liu, S.; Wang, R.; Guo, J.; Ma, X. Liquid Metal-Based Epidermal Flexible Sensor for Wireless Breath Monitoring and Diagnosis Enabled by Highly Sensitive SnS_2 Nanosheets. *Research* **2021**, *2021*, 9847285.
(25) Elbourne, A.; Cheeseman, S.; Atkin, P.; Truong, N. P.; Syed, N.; Zavabeti, A.; Mohiuddin, M.; Esrafilzadeh, D.; Cozzolino, D.; McConville, C. F.; Dickey, M. D.; Crawford, R. J.; Kalantar-Zadeh, K.; Chapman, J.; Daeneke, T.; Truong, V. K. Antibacterial Liquid Metals: Biofilm Treatment via Magnetic Activation. *ACS Nano* **2020**, *14* (1), 802−817.
(26) Cheeseman, S.; Elbourne, A.; Kariuki, R.; Ramarao, A. V.; Zavabeti, A.; Syed, N.; Christofferson, A. J.; Kwon, K. Y.; Jung, W.; Dickey, M. D.; Kalantar-Zadeh, K.; McConville, C. F.; Crawford, R. J.; Daeneke, T.; Chapman, J.; Truong, V. K. Broad-Spectrum Treatment of Bacterial Biofilms Using Magneto-Responsive Liquid Metal Particles. *J. Mater. Chem. B* **2020**, *8* (47), 10776−10787.
(27) Kwon, K. Y.; Cheeseman, S.; Frias-De-Diego, A.; Hong, H.; Yang, J.; Jung, W.; Yin, H.; Murdoch, B. J.; Scholle, F.; Crook, N.; Crisci, E.; Dickey, M. D.; Truong, V. K.; Kim, T.-i. A Liquid Metal Mediated Metallic Coating for Antimicrobial and Antiviral Fabrics. *Adv. Mater.* **2021**, *33* (45), 2104298.
(28) Sun, X.; Sun, M.; Liu, M.; Yuan, B.; Gao, W.; Rao, W.; Liu, J. Shape Tunable Gallium Nanorods Mediated Tumor Enhanced Ablation through Near-Infrared Photothermal Therapy. *Nanoscale* **2019**, *11* (6), 2655−2667.
(29) Marletta, M. A. Nitric Oxide Synthase Structure and Mechanism. *J. Biol. Chem.* **1993**, *268* (17), 12231−12234.
(30) Lowenstein, C. J.; Padalko, E. iNOS (NOS2) at a Glance. *J. Cell Sci.* **2004**, *117* (14), 2865−2867.
(31) MacMicking, J.; Xie, Q.-W.; Nathan, C. Nitric Oxide and Macrophage Function. *Annu. Rev. Immunol.* **1997**, *15* (1), 323−350.
(32) Duffield, J. S. The Inflammatory Macrophage: A Story of Jekyll and Hyde. *Clin. Sci.* **2003**, *104* (1), 27−38.
(33) Coleman, J. W. Nitric Oxide in Immunity and Inflammation. *Int. Immunopharmacol.* **2001**, *1* (8), 1397−1406.
(34) Bogdan, C. Nitric Oxide and the Immune Response. *Nat. Immunol.* **2001**, *2* (10), 907−916.
(35) Hobbs, A. J.; Higgs, A.; Moncada, S. Inhibition of Nitric Oxide Synthase as a Potential Therapeutic Target. *Annu. Rev. Pharmacol. Toxicol.* **1999**, *39* (1), 191−220.
(36) Cohen, J. The Immunopathogenesis of Sepsis. *Nature* **2002**, *420* (6917), 885−891.
(37) Chung, H.-T.; Pae, H.-O.; Choi, B.-M.; Billiar, T. R.; Kim, Y.-M. Nitric Oxide as a Bioregulator of Apoptosis. *Biochem. Biophys. Res. Commun.* **2001**, *282* (5), 1075−1079.
(38) Merly, L.; Smith, S. L. Murine Raw 264.7 Cell Line as an Immune Target: Are We Missing Something? *Immunopharmacol. Immunotoxicol.* **2017**, *39* (2), 55−58.
(39) Bright, N. A.; Davis, L. J.; Luzio, J. P. Endolysosomes Are the Principal Intracellular Sites of Acid Hydrolase Activity. *Curr. Biol.* **2016**, *26* (17), 2233−2245.
(40) Yang, R.-B.; Mark, M. R.; Gray, A.; Huang, A.; Xie, M. H.; Zhang, M.; Goddard, A.; Wood, W. I.; Gurney, A. L.; Godowski, P. J. Toll-Like Receptor-2 Mediates Lipopolysaccharide-Induced Cellular Signalling. *Nature* **1998**, *395* (6699), 284−288.
(41) Nagatoshi, F.; Kazuo, K. Macrophages in Inflammation. *Curr. Drug Targets Inflamm. Allergy* **2005**, *4* (3), 281−286.
(42) Heo, S.-J.; Yoon, W.-J.; Kim, K.-N.; Ahn, G.-N.; Kang, S.-M.; Kang, D.-H.; Affan, A.; Oh, C.; Jung, W.-K.; Jeon, Y.-J. Evaluation of Anti-Inflammatory Effect of Fucoxanthin Isolated from Brown Algae in Lipopolysaccharide-Stimulated RAW 264.7 Macrophages. *Food Chem. Toxicol.* **2010**, *48* (8−9), 2045−2051.
(43) Fan, G.-W.; Gao, X.-M.; Wang, H.; Zhu, Y.; Zhang, J.; Hu, L.-M.; Su, Y.-F.; Kang, L.-Y.; Zhang, B.-L. The Anti-Inflammatory Activities of Tanshinone IIA, an Active Component of TCM, are Mediated by Estrogen Receptor Activation and Inhibition of iNOS. *J. Steroid Biochem. Mol. Biol.* **2009**, *113* (3−5), 275−280.
(44) Shih, M.-F.; Cheng, Y.-D.; Shen, C.-R.; Cherng, J.-Y. A Molecular Pharmacology Study into the Anti-Inflammatory Actions of *Euphorbia Hirta* L. On the LPS-Induced RAW 264.7 Cells through Selective iNOS Protein Inhibition. *J. Nat. Med.* **2010**, *64* (3), 330−335.
(45) Sampaio, A. L. F.; Jesmond, D.; Vincenzo, B.; Fulvio, D. A.; Mauro, P.; Carmen, W. Biphasic Modulation of NOS Expression, Protein and Nitrite Products by Hydroxocobalamin Underlies its Protective Effect in Endotoxemic Shock: Downstream Regulation of

https://doi.org/10.1021/acsnano.1c10981
ACS Nano XXXX, XXX, XXX−XXX

COX-2, IL-1β, TNF-α, IL-6, and HMGB1 Expression. *Mediators Inflamm.* **2013**, *2013*, 741804.
(46) Eshelman, M. A.; Matthews, S. M.; Schleicher, E. M.; Fleeman, R. M.; Kawasawa, Y. I.; Stumpo, D. J.; Blackshear, P. J.; Koltun, W. A.; Ishmael, F. T.; Yochum, G. S. Tristetraprolin Targets NOS2 Expression in the Colonic Epithelium. *Sci. Rep.* **2019**, *9*, 14413.
(47) Lee, J.; Ryu, H.; Ferrante, R. J.; Morris, S. M.; Ratan, R. R. Translational Control of Inducible Nitric Oxide Synthase Expression by Arginine Can Explain the Arginine Paradox. *Proc. Natl. Acad. Sci. U. S. A.* **2003**, *100* (8), 4843−4848.
(48) Yin, H.-Y.; Gao, J.-J.; Chen, X.; Ma, B.; Yang, Z.-S.; Tang, J.; Wang, B.-W.; Chen, T.; Wang, C.; Gao, S.; Zhang, J.-L. A Gallium(III) Complex that Engages Protein Disulfide Isomerase A3 (PDIA3) as an Anticancer Target. *Angew. Chem., Int. Ed.* **2020**, *59* (45), 20147−20153.
(49) Boye, E.; Grallert, B. eIF2α Phosphorylation and the Regulation of Translation. *Curr. Genet.* **2020**, *66* (2), 293−297.
(50) Qi, J.; Qian, K.; Tian, L.; Cheng, Z.; Wang, Y. Gallium(III)-2-Benzoylpyridine-Thiosemicarbazone Complexes Promote Apoptosis through Ca^{2+} Signaling and ROS-Mediated Mitochondrial Pathways. *New. J. Chem.* **2018**, *42* (12), 10226−10233.
(51) Beriault, R.; Hamel, R.; Chenier, D.; Mailloux, R. J.; Joly, H.; Appanna, V. D. The Overexpression of Nadph-Producing Enzymes Counters the Oxidative Stress Evoked by Gallium, an Iron Mimetic. *Biometals* **2007**, *20* (2), 165−176.
(52) Seligman, P. A.; Moran, P. L.; Schleicher, R. B.; Crawford, E. D. Treatment with Gallium Nitrate: Evidence for Interference with Iron Metabolism in Vivo. *Am. J. Hematol.* **1992**, *41* (4), 232−240.
(53) Olakanmi, O.; Britigan, B. E.; Schlesinger, L. S. Gallium Disrupts Iron Metabolism of Mycobacteria Residing within Human Macrophages. *Infect. Immun.* **2000**, *68* (10), 5619−5627.
(54) Stonyte, V.; Boye, E.; Grallert, B. Regulation of Global Translation During the Cell Cycle. *J. Cell Sci.* **2018**, *131* (17), jcs220327.
(55) Dever, T. E. Gene-Specific Regulation by General Translation Factors. *Cell* **2002**, *108* (4), 545−556.
(56) Khan, M. A.; Khan, M. J. Nano-Gold Displayed Anti-Inflammatory Property via NF-kB Pathways by Suppressing COX-2 Activity. *Artif. Cells Nanomed. Biotechnol.* **2018**, *46*, 1149−1158.
(57) Franková, J.; Pivodová, V.; Vágnerová, H.; Juráňová, J.; Ulrichová, J. Effects of Silver Nanoparticles on Primary Cell Cultures of Fibroblasts and Keratinocytes in a Wound-Healing Model. *J. Appl. Biomater. Funct.* **2016**, *14* (2), 137−142.
(58) Prasad, S. R.; Elango, K.; Chellakumari, S.; Dharani, S. Preparation, Characterization and Anti-Inflammatory Activity of Chitosan Stabilized Silver Nanoparticles. *Res. J. Pharm. Dosage Forms Technol.* **2013**, *5* (3), 161−167.
(59) Agarwal, H.; Shanmugam, V. A Review on Anti-Inflammatory Activity of Green Synthesized Zinc Oxide Nanoparticle: Mechanism-Based Approach. *Bioorg. Chem.* **2020**, *94*, 103423.
(60) Griess, P. Bemerkungen zu der Abhandlung der HH. Weselsky und Benedikt Ueber einige Azoverbindungen. *Ber. Dtsch. Chem. Ges.* **1879**, *12* (1), 426−428.
(61) Livak, K. J.; Schmittgen, T. D. Analysis of Relative Gene Expression Data Using Real-Time Quantitative PCR and the $2^{-\Delta\Delta CT}$ Method. *Methods* **2001**, *25* (4), 402−408.

https://doi.org/10.1021/acsnano.1c10981
ACS Nano XXXX, XXX, XXX−XXX